J. Condensed Matter Nucl. Sci. 24 (2017) 202–213

Research Article

Collaborative Examination on Anomalous Heat Effect Using Nickel-based Binary Nanocomposites Supported by Zirconia

Akira Kitamura*,†, Akito Takahashi, Koh Takahashi, Reiko Seto and Yuki Matsuda

Technova Inc., 100-0011 Tokyo, Japan

Yasuhiro Iwamura, Takehiko Itoh and Jirohta Kasagi

Research Center for Electron Photon Science, Tohoku University, 982-0826 Sendai, Japan

Masanori Nakamura, Masanobu Uchimura and Hidekazu Takahashi

Research Division, Nissan Motor Co. Ltd., 237-8523 Kanagawa, Japan

Tatsumi Hioki and Tomoyoshi Motohiro

Green Mobility Research Institute, Institutes of Innovation for Future Society, Nagoya University, 464-8603 Nagoya, Japan

Yuichi Furuyama

Graduate School of Maritime Sciences, Kobe University, 658-0022 Kobe, Japan

Masahiro Kishida

Graduate School of Engineering, Kyushu University, 819-0395 Kyushu, Japan

Abstract

Hydrogen isotope absorption by nickel-based binary nanocomposite samples has been examined in collaborative work in the new NEDO MHE project. The samples tested so far include Pd0.044Ni0.31Zr0.65 (“PNZ3” and re-calcined “PNZ3r”) and Cu0.044Ni0.31Zr0.65 (“CNZ5”). Material characterization by XRD and STEM/EDS has revealed the (continued in next page)
 ISSN 2227-3123

Keywords: Anomalous excess heat, Binary Ni-based nano-particles, Elevated temperature, Large hydrogen absorption, Melt-spinning samples, ZrO_2 supporter

*E-mail: kitamuraakira3@gmail.com.

†Also at: Graduate School of Maritime Sciences, Kobe University, 658-0022 Kobe, Japan.

 ISSN 2227-3123

(continued from p. 202) existence of crystalline phases of $NiZr_2$, ZrO_2, etc., and nano-meter size structures of binary Pd/Ni or Cu/Ni composites in ZrO_2 supporter. All samples at elevated temperatures (200–300°C) showed anomalous heat evolution with excess power of 5–10 W for periods of several days, which corresponded to excess energy of 5 keV/atom-D(H) or 0.5 GJ/mol-D(H). This anomalous heat generation phenomenon could be the basis for practical, carbon-free energy devices that do not produce hard radiations.

1. Introduction

There has been increasing interest in experiments with hydrogen gas charged nickel-based nano-composite samples for excess energy generation, owing to the higher availability of nickel compared to palladium. A Ni–Cu–Mn alloy thin wire, for example, has been examined extensively by Celani et al. [1]. In addition, a number of entrepreneurs are publicizing their own "products" of nano-fabricated samples on web sites with undisclosed details, and therefore with little scientific corroboration (e.g., [2,3]). Among them, replication experiments of the Rossi-type reactors have been performed by several researchers [4–7], which seemingly show considerable reproducibility of the Rossi method. However, little is known about the accuracy of the calorimetry or the mechanism of the claimed anomalously large energy production.

As reviewed in Ref. [8], the 8-year-long (2008–2015) series of studies on anomalous heat effects by interaction of metal nano-particles and D(H)-gas under the collaboration of Technova Inc. and Kobe University has become the basis of a national research effort sponsored by NEDO, which is hoped to lead to a new CO_2 free energy source. The new NEDO project on New Metal–Hydrogen Energy was started in October 2015 with a collaboration of six Japanese institutions, one of which the individual author of the present paper belongs to. The first result by the project is reported in this paper.

In the present work, hydrogen isotope absorption by nickel-based nano-composite samples has been examined in a collaboration using the experimental apparatus installed at Kobe University [8,9,11,13] in order to share scientific understanding of the anomalous heat effects both at room temperature (RT) and elevated temperatures. The system [9] has a reaction chamber with the capacity to hold a sample of 500 cm^3, and a flow-calorimetry system capable of working at elevated temperatures up to 300°C with use of a liquid hydrocarbon coolant. The samples tested so far include $Pd_{0.044}Ni_{0.31}Zr_{0.65}$ ("PNZ3" and re-calcined "PNZ3r") and $Cu_{0.044}Ni_{0.31}Zr_{0.65}$ ("CNZ5"), whose D(H)-absorption/heat-generation characteristics are discussed in the present paper.

2. Characteristics of Samples

The samples are an amorphous mixture of the metal elements prepared by the melt spinning method, and calcined in air at a temperature of 450°C for 69–100 h, during which preferential oxidation of Zr to ZrO_2 is expected with a consequent formation of binary-nano-particles of Pd/Ni or Cu/Ni embedded in it. The sample composition and calcination conditions are summarized in Table 1. The sample designated PNZ3r was subjected to the hydrogen isotope absorption runs at Kobe University, and subsequently re-calcined in air at 450°C for 200 h. The oxygen content was evaluated from the weight difference before and after the calcination/re-calcination. The samples CNZ5s and PNZ4s are from the same lot as CNZ5 and PNZ4, respectively. They were subjected to absorption runs at Tohoku University, whose results are presented in another paper by Iwamura et al. [10]. Atomic ratios of Pd/Ni or Cu/Ni were chosen to be ca. 1/7 based on the experience of the Technova–Kobe contribution [8,9,11,13] to the present work.

ICP-AES and XRD analyses were done at Nissan Motor Co. Ltd., Kyushu University, and Nagoya University independently. Many interesting features including crystalline phases of $NiZr_2$, ZrO_2, etc. have been revealed, which will be published independently elsewhere. STEM/EDS analyses done at Kobe University showed features of nano-structure of the samples. Two examples are shown in Fig. 1, showing a tendency of agglomeration of Pd and Ni

Table 1. Sample composition and sintering conditions.

Sample name	Tested at	Weight (g)	Molar fraction (%)					Duration of oxidation at 450°C (h)
			Cu	Pd	Ni	Zr	O	
PNZ3	Kobe	95.5	–	3.5	24.5	52.0	20.0	100
PNZ3r	Kobe	113.2	–	1.7	11.6	24.5	62.3	200
CNZ5	Kobe	130.4	1.7	–	11.6	24.5	62.3	60
CNZ5s	Sendai	130.0						
PNZ4	Kobe	109.4	–	3.6	25.2	53.4	17.8	60
PNZ4s	Sendai	109.4						

particles together during D_2 absorption, runs followed by re-calcination and repeated absorption runs. Some features deduced from the pictures are summarized in Table 2.

3. Experimental Procedure

A schematic of the absorption-calorimetry system C_1 is shown in Fig. 2. Refer to [9] for detailed description of the system. Calibration of the flow calorimetry with a flow rate of 10 ml/min was done using 1-mm-diam. zirconia balls.

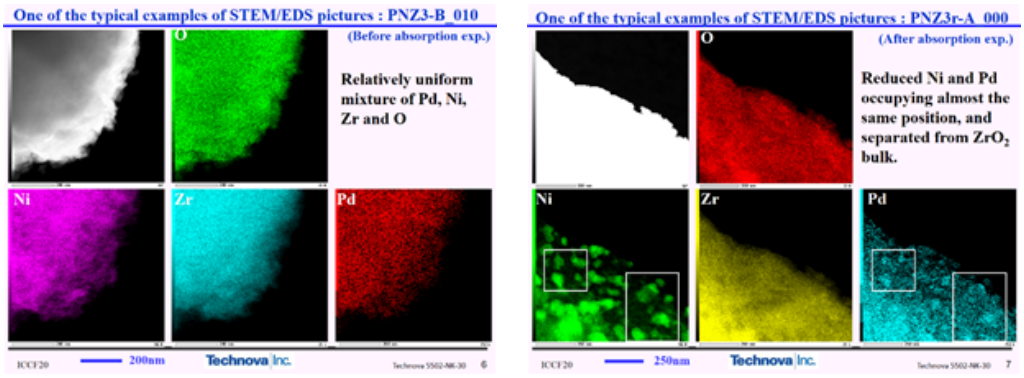

(a) **(b)**

Figure 1. Two examples of STEM/EDS.

Table 2. Some features perceived in STEM/EDS pictures.

PNZ3	Amorphous ribbon calcined at 450°C for 100 h	•Mostly, relatively uniform mixture of Pd, Ni, Zr and O, but partly nonuniform distribution of Ni and Pd is recognized •Most Pd and Ni atoms occupy the same position •After absorption runs, $NiZr_2$ decreased, and ZrO_2 increased, and some reduced Ni atoms form a block
PNZ3r	Used PNZ3 re-calcined at 450°C for 200 h	•The assumed majority is $ZrO_2 + NiO + PdO$ •O atoms have increased •NiO and PdO appear to be separated from ZrO_2 •Nonuniform distribution of Ni and Pd atoms developed further •After absorption runs, NiO and PdO appear to be reduced

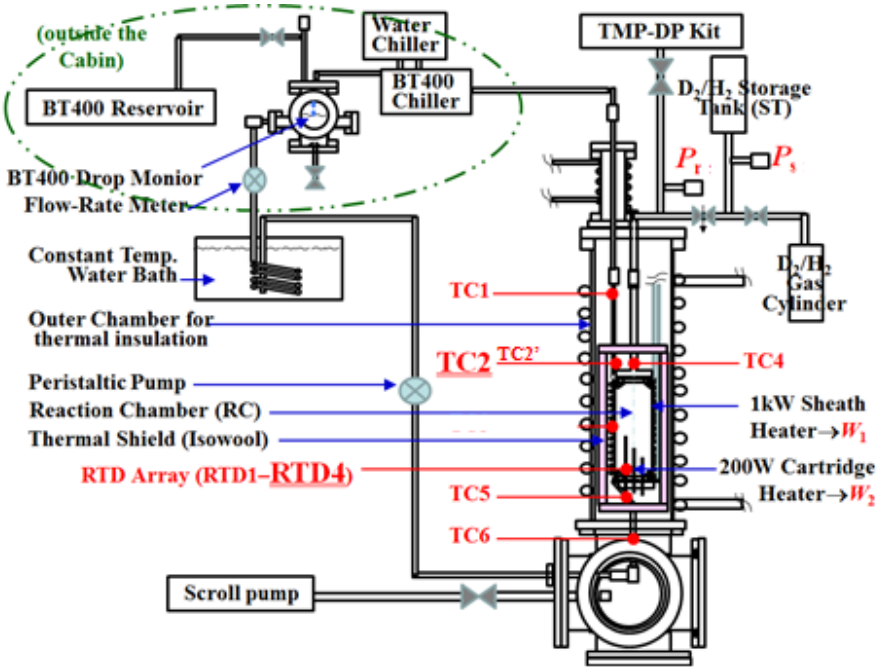

Figure 2. Experimental apparatus: Hydrogen isotope absorption-calorimetry system.

The heat conversion coefficient, $dT_{C2}/dW = 2.7°C/W$ or $1.44°C/W$, was obtained at RT or in the temperature range from 200 to 300°C, respectively. The heat recovery rate was calculated as

$$R_h = F\rho C(T_{C2} - T_{C6})/(W_1 + W_2), \quad (1)$$

where F, ρ and C are the flow rate, the mass density and the specific heat capacity, respectively, of the coolant BarrelTherm-400 (BT400), Matsumura Oil Co. Ltd., and W_1 and W_2 the outer sheath (#1) and the inner cartridge (#2) heater power, respectively. The mean value of $R_h = 0.8$ is a little lower than in the case of the C_1 system before the addition of the #2 heater due to increased loss of heat through the lead wire. The calibration run also serves as a control run giving reference temperatures, the flow rate of BT400 and heater power for foreground runs using the Ni-based samples. Comparing the temperatures in the foreground and background runs, the excess power is calculated using $dT_{C2}/dW = 2.7°C/W$ or $1.44°C/W$ in RT runs or elevated temperature runs, respectively.

As an example of foreground runs, the temperature and D(H)-loading history in the deuterium-filled PNZ3 runs, D-PNZ3#1 through D-PNZ3#3, and the protium-filled run, H-PNZ3#4, are shown in Fig. 3. Every run has several phase-runs with different combinations of the nominal input power (W_1, W_2) in watts, as indicated on the extreme right. The run #n is separated by a vacuum baking phase at the end of the preceding run #(n-1). The hydrogen loading ratio is also plotted in the figure. That is, $L_M \equiv$ D(H)/M, defined as the number of D (or H) atom lost from the gas phase inside the reaction chamber (RC) divided by the number of metal atoms M, where M stands for both for Pd and Ni atoms. That is to say, M denotes (7Ni + Pd)/8 for PNZ3 and PNZ3r, Ni for CNZ5, respectively. The term L_M is calculated from the pressure of RC and of the storage tank (ST), P_r and P_s, respectively, and their volumes with a correction for the temperature change based on the Boyle–Charles' law.

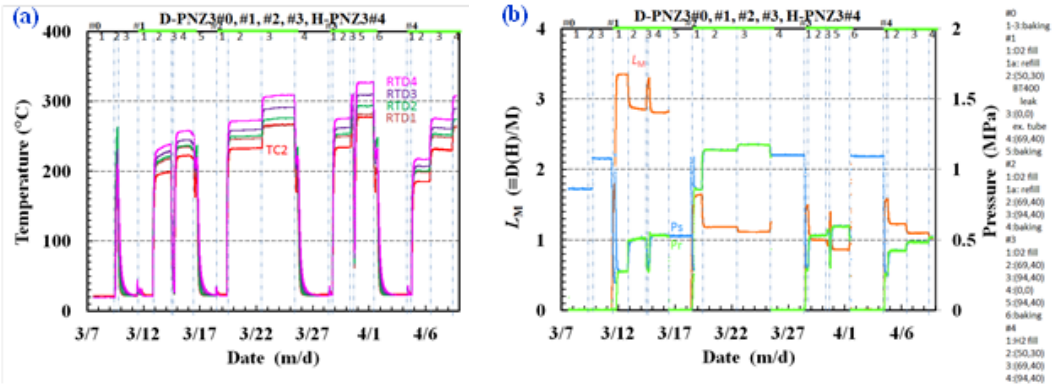

Figure 3. Temperature (a) and D(H)-loading and (b) history of PNZ3 runs.

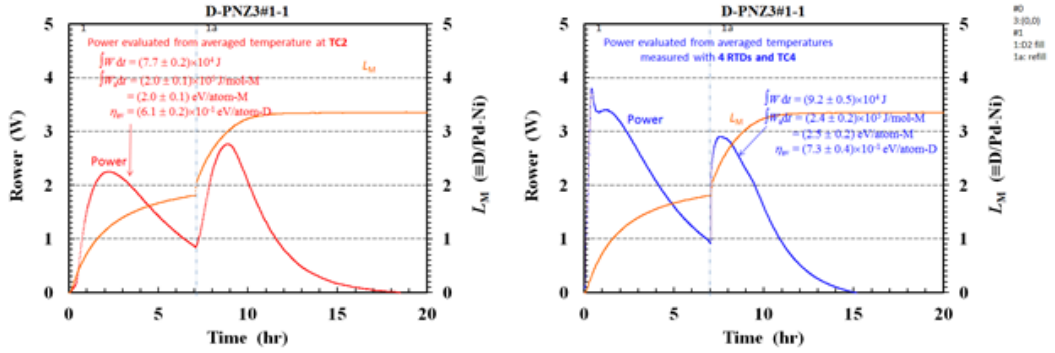

Figure 4. Initial burst of heat recorded on (a) TC2 and (b) RTDav in the PNZ3#1-1 phase at RT.

4. Results and Discussion

4.1. Heat evolution in RT phases

4.1.1. *PNZ3*

Let us first discuss the PNZ3 sample. In the PNZ3#1-1 phase, when the annealed virgin PNZ3 sample is exposed to hydrogen isotope gas, large initial bursts of heat are observed on the TC and RTD traces. The power recorded on the TC2 and RTDs are shown in Fig. 4. The latter is calculated by using the average temperature of those on RTD1 through RTD4 and TC4, which we call RTDav collectively hereafter. The reason why they have two peaks is simply because the ST was replenished to the initial high pressure at about 7 h after initiation of the run, which increased the heat evolution rate as a result of the increased flow rate of D_2 due to the increased pressure in the ST. temperature change based on the Boyle–Charles' law.

The humps are time-integrated in the #1-1 phase to calculate the emerging energy per absorbent atom,

$$E_{\rm a} = \int_0^{T_1} W_{\rm a} {\rm d}t, \tag{2}$$

where $W_{\rm a}$ is the power per adsorbent atom M, and T_1 is the duration of the #1-1 phase. The energy $E_{\rm a}$ is divided by the saturation value of $L_{\rm M}$ to give the specific sorption energy averaged in the #1-1 phase,

$$\eta_{\rm av} = \frac{E_{\rm a}}{L_{\rm M}}. \tag{3}$$

These are calculated to be $E_{\rm a} = (2.0 \pm 0.1)$ eV/atom-M and $\eta_{\rm av} = 0.61 \pm 0.02$ eV/atom-D for TC2, or $E_{\rm a} = (2.5 \pm 0.2)$ eV/atom-M and $\eta_{\rm av} = 0.73 \pm 0.04$ eV/atom-D for RTDav.

It should be stressed that not only Pd but also Ni atoms are contributing to absorption of hydrogen isotopes at RT in the present binary nano-composite system supported by zirconia; this is regarded as a catalytic effect of the minor constituent Pd. The values of $E_{\rm a} = 2.0$ to 2.6 eV/atom-M and $\eta_{\rm av} = 0.6$ to 0.7 eV/atom-D are rather large in view of the hydrogen absorption energy of about 0.2 eV/atom-Pd and 0.22 eV/atom-D for bulk crystalline Pd. However, this is quite reasonable when we take into account that the XRD analysis of the virgin PNZ3 sample showed the existence of $NiZr_2$ and NiO [11]. Possible reactions to be taken into account other than hydrogen absorption/adsorption by Pd/Ni particles could be oxygen pickup reactions,

$$\text{PdO+D}_2(\text{H}_2) \rightarrow \text{Pd+D}_2\text{O}(\text{H}_2\text{O}) + 1.77(1.63)\,\text{eV/atom-Pd}, \tag{4}$$

$$\text{NiO+D}_2(\text{H}_2) \rightarrow \text{Ni+D}_2\text{O}(\text{H}_2\text{O}) + 0.176(0.033)\,\text{eV/atom-Ni} \tag{5}$$

and the hydrogenation reaction [12] with H replaced by D,

$$\text{NiZr}_2 + (4.5/2)\text{H}_2 \rightarrow \text{ZrH}_2 + \text{ZrNiH}_{2\ 5} + 2.85\,\text{eV/atom-Ni}\,(0.63\,\text{eV/atom-H}). \tag{6}$$

The contribution of these reactions (4)–(6) can account for the large values of $E_{\rm a}$ and $\eta_{\rm av}$, and also of $L_{\rm M}$ >3 in the #1-1 phase. A quantitatively exact comparison of the observed $E_{\rm a}$ and $\eta_{\rm av}$ with the above reaction energies, or a discussion of the existence of anomalous reaction such as nuclear ones, will be possible after the fractional amounts of these phases, $NiZr_2$, NiO and PdO, are known exactly.

As shown in Fig. 3, $L_{\rm M}$ is reduced to below 1.6 in the #2-1 and later phases after evacuation and baking in the #1-5 phase. The variations of $L_{\rm M}$, $E_{\rm a}$ and $\eta_{\rm av}$ in the #n-1 RT phases ($n = 1$ to 5) evaluated at TC2 are shown in Fig. 5, and compared with those evaluated from the averaged values of the temperatures recorded on RTDav. Only the #1-1 phase has the exceptionally large values of $L_{\rm M}$, $E_{\rm a}$ and $\eta_{\rm av}$. This appears to show that the formation of very stable ZrH_2 and possibly oxygen pickup reactions (4) and (5) only occur in the #1-1 phase, and are irreversible, or the ZrH_2 does not lose H during the evacuation and baking at temperatures around 300°C. (Hereafter, H stands for both protium and deuterium, unless explicitly declared.)

As can be seen in Fig. 3, $L_{\rm M}$ depends on temperature rather strongly in the #2-1 and later phases. However, almost the same value of $L_{\rm M}$ is recovered in the #n-1 phases (n >2). The absorption/desorption is reversible and repeatable. However, $L_{\rm M}$ cannot be decreased below about 1.0 under elevated temperatures up to 330°C. In these phases, formation of hydrides PdH_x/NiH_x and $ZrNiH_{2\ 5}$ could be responsible for the hydrogen absorption. The facts mentioned above imply that hydrogen retention of either PdH_x/NiH_x or $ZrNiH_{2\ 5}$ is dependent strongly on temperature in the range below 330°C, while the other ($ZrNiH_{2\ 5}$ or PdH_x/NiH_x) retains H in this temperature range with $L_{\rm M} \sim 1$.

The specific absorption energies $E_{\rm a}$ and $\eta_{\rm av}$ in the phases #n-1 (n >1) are also large compared with those for the bulk crystalline Pd mentioned earlier. The reason for this could be an anomalous effect including a nuclear one

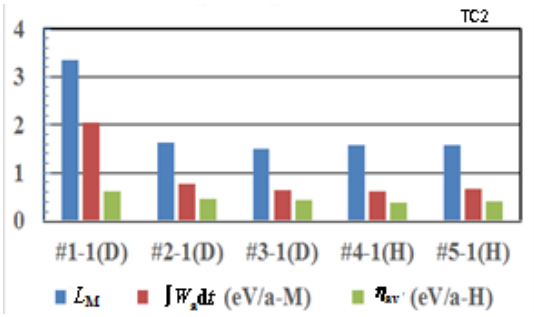

(a)

		#1-1(D)	#2-1(D)	#3-1(D)	#4-1(H)	#5-1(H)
L_M		3.35E+00	1.64E+00	1.50E+00	1.59E+00	1.57E+00
TC2						
$\int W_a dt$	(eV/a-M)	2.04E+00	7.68E-01	6.48E-01	6.17E-01	6.63E-01
η_{av}	(eV/a-H)	6.09E-01	4.67E-01	4.32E-01	3.89E-01	4.22E-01
RTDav						
$\int W_a dt$	(eV/a-M)	2.45E+00	7.74E-01	7.22E-01	6.91E-01	6.74E-01
η_{av}	(eV/a-H)	7.31E-01	4.70E-01	4.81E-01	4.35E-01	4.29E-01

(b)

Figure 5. Loading ratio and output energy in the first phases at RT (PNZ3#n-1) evaluated at TC2 (*left*), which are compared in the right table with those at RTDav.

under hydrogen absorption of Pd/Ni nano-particles. To reach this conclusion, however, the contribution of $ZrNiH_{2.5}$ formation to the absorption energies has to be evaluated quantitatively.

It should also be emphasized here that the values of absorption energies evaluated from TC2 and from RTDav agree within an error of about 20%. The heat evolution, or the sample distribution, is rather uniform in the present system. This justifies the use of RTDav in the calculation of excess power in the elevated temperatures discussed in Section 4.2.

4.1.2. *PNZ3r and CNZ5*

Both the PNZ3r and CNZ5 samples showed very little absorption in the RT phases: $L_M \sim 0.1$ with $E_a \sim 0.06$ eV/atom-M and $\eta_{av} \sim 0.6$ eV/atom-D in PNZ3r#1-1, and $L_M \sim 0.2$ with $E_a \sim 0.1$ eV/atom-M and $\eta_{av} \sim 0.5$ eV/atom-H in CNZ5#1-1. It is easy to understand the small values in the sample CNZ5#1-1, since it is established that both Ni and Cu particles do not absorb much hydrogen at RT, in contrast to Pd. The non-zero values of these variables could be related to this sample's ability to absorb substantial amounts of hydrogen at elevated temperatures, as will be discussed in Section 4.2. In other words, the very small values of L_M at RT is simply a result of the Arrhenius law for absorption with an activation energy of around 0.04 eV as inferred by the temperature dependence of the absorption by this sample.

However, the small values in the PNZ3r#1-1 are difficult to understand, since the sample contains Pd. This sample was the PNZ3 re-calcined after finishing the PNZ3#4 run. The re-calcination was done in air at a temperature of 450°C for 200 h, during which hydrogenated Pd/Ni particles should have been reduced and oxidized. The sample appears to have suffered from agglomeration and/or segregation of Pd/Ni particles as seen in Fig. 1. It seems that the change of properties has led to the loss of hydrogen absorption activity of Pd/Ni. The non-zero values here again could be related to the hydrogen absorption property at elevated temperatures, discussed in Section 4.2.

4.2. Excess power evolution in the elevated temperature phases

In the elevated temperature phases, where L_M takes the saturated values depending on the temperature, the temperatures T_{C2} at TC2 and T_{RTDav} are compared with the reference ones in the control run. The difference, if any, is divided by the conversion rate, dT/dW, and the number of metal atoms M to give the specific excess power, W_{ex} (W/atom-M). This is integrated to give the specific excess energy, E_{ex} (eV/atom-M), which is divided by the increment of $\Delta L_M(T_j)$ during each phase j with duration of T_j to give the specific sorption energy, $\eta_{av,j}$ (eV/atom-H), where the absolute

value $|\Delta L_{\rm M}(T_j)|$ is adopted in the denominator. This means that both absorption and desorption are considered to be effective ways to generate anomalous excess power.

$$E_{\rm ex} = \int_0^t W_{\rm ex} {\rm d}t, \tag{7}$$

$$\eta_{{\rm av},i} = \frac{\int_{t-T_j}^{t} W_{\rm ex} {\rm d}t}{|\Delta L_{\rm M}\,(T_j)\,|}. \tag{8}$$

Another evaluation of the specific sorption energy, $\eta_{\rm t}$, (eV/atom-H), might be possible by dividing $E_{\rm ex}$ in each run #n by the total amount of hydrogen isotopes having participated in the absorption $L_{{\rm M},n}$ in each run #n, and by summing up over the runs,

$$\eta_t = \sum_n \frac{E_{\rm ex} {\rm d}t}{L_{M,n}}. \tag{9}$$

Below in the present paper, $T_{\rm RTDav}$ is used to calculate excess power. This is because TC2 had a problem caused by contact failure at elevated temperatures. The use of $T_{\rm RTDav}$ is justified by the approximate equality of this and $T_{\rm C2}$ shown in Fig. 5, as mentioned earlier.

4.2.1. *PNZ3*

Variation of the temperature at RTDav (red) and after correction for the fluctuation of the flow rate of BT400 (green) are shown in Fig. 6(a) in comparison with the reference temperature at RTDav in ZrO_2 calibration run (black). The loading ratio $L_{\rm M}$ (orange) is also shown in the figure. As discussed in Section 4.1.1, the loading ratio $L_{\rm M}$ is rather high, possibly due to the formation of ZrH_2 (6) and oxygen pickup reactions (4) and (5), and is reduced to 1.6 in the #2-1 and later phases, when the formation of hydrides PdH_x/NiH_x and $ZrNiH_{2\ 5}$ could be responsible for the absorption.

Figure 6(b) shows the specific excess power $W_{\rm ex}$ after additional correction for input heater power (brown), the integrated excess energy $E_{\rm ex}$ (black square) and the specific sorption energy $\eta_{{\rm av},j}$ (blue circle). In almost all phases the corrected temperature is larger than the reference one, and therefore the excess power is positive. The maximum excess power is about 10 W in the PNZ3#3-3 and #3-5 phases with the input power of $(W_1, W_2) =$ (94 W, 40 W), while the measurement error evaluated in various runs using blank samples is $\pm 1.5\%$ of the input power, or ± 2 W in the present case. The PNZ3#3-4 phase with (0 W, 0 W) was successfully run to confirm the reproducibility of $L_{\rm M} = 1.6$ at RT.

The integrated specific excess energy $E_{\rm ex}$ is several tens of eV/atom-M in each phase, and amounts to $E_{\rm ex}\sim 1.8\times 10^2$ eV/atom-M (1.8×10^1 MJ/mol-M) at the end of the #4 run. The specific sorption energy defined by Eq. (8), $\eta_{{\rm av},j}$, is in the range from 3.2×10^2 eV/atom-H to 1.6×10^1 keV/atom-H. These are very large values that cannot be explained by any chemical processes caused by outer shell electrons having binding energies of the order of 10 eV. If we evaluate the specific sorption energy as defined by Eq. (9), we obtain $\eta_{\rm t}\sim 9.8\times 10^1$ eV/atom-H. This is again one order of magnitude greater than the chemical one. We have to consider the possibility of nuclear origin for the energy production in the present system.

4.2.2. *CNZ5*

Similarly, the same variables are plotted in Fig. 7(a) and (b) for the CNZ5 sample. In this sample, only runs with protium gas were tested. This sample also generates excess power of up to 8 W, with $\eta_{{\rm av},j}$ ranging from 2.4×10^{-2}

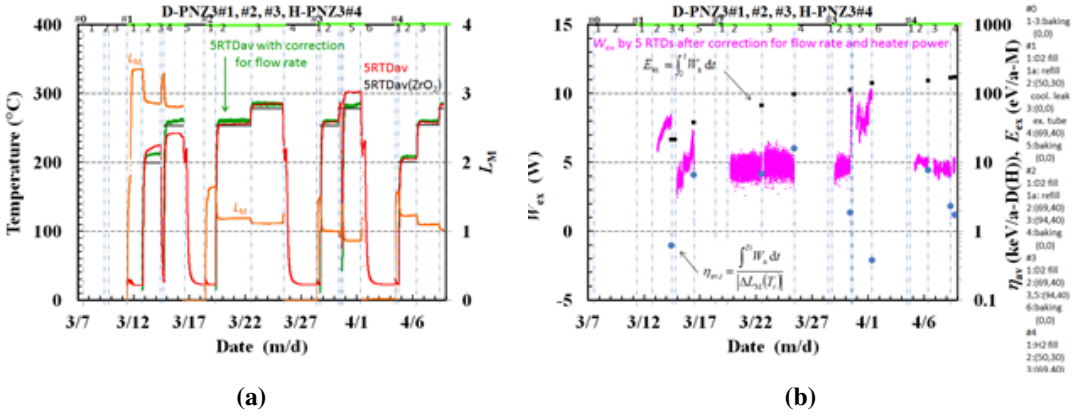

(a) **(b)**

Figure 6. (a) Temperature at RTDav (*red*), the temperature corrected for flow rate fluctuation (*green*), the reference temperature at RTDav (*black*), and the loading ratio L_{M} (*orange*) in PNZ3#1 through PNZ3#4 runs. (b) The specific excess power W_{ex} (*purple*), the integrated excess energy E_{ex} (*black square*) and the specific sorption energy $\eta_{\mathrm{ex},j}$ (*blue circle*).

to 2.7 keV/atom-H and E_{ex}∼5.1× 10^1 eV/atom-M (5.1 MJ/mol-M) at the end of the #1 run. The values are rather modest, though not explainable by any known chemical reaction energy.

Very little hydrogen is absorbed in the #1-1 phase, until it starts to absorb a substantial amount of hydrogen at elevated temperatures of up to 200°C. The absorption characteristics of this sample resemble those of the CNS2 sample [13]. The CNS2 is a $CuNi_7$ nano-composite sample supported by mesoporus-SiO_2. The sample showed no absorption at RT, and absorbed protium up to L_{M}∼0.9 in the elevated temperature phases up to T∼200°C. It also produced excess power of W_{ex}∼10 W, E_{ex} = 3.8× 10^2 eV/atom-M and η_{av}∼1.5× 10^4 eV/atom-H in the phases where L_{M} is saturated. It is inferred therefore that the absorption in CNZ5#1-2 phase and the excess power production is caused by Ni nano-particles with the catalyzing effect of Cu. A small difference between CNS2 and CNZ5 in the absorption at RT, together with the difference of factor 2 in L_{M}, might be a result of the difference in the supporting material. In the present CNZ5 sample, the hydrogenation reaction (6) might be contributing. However, only a small

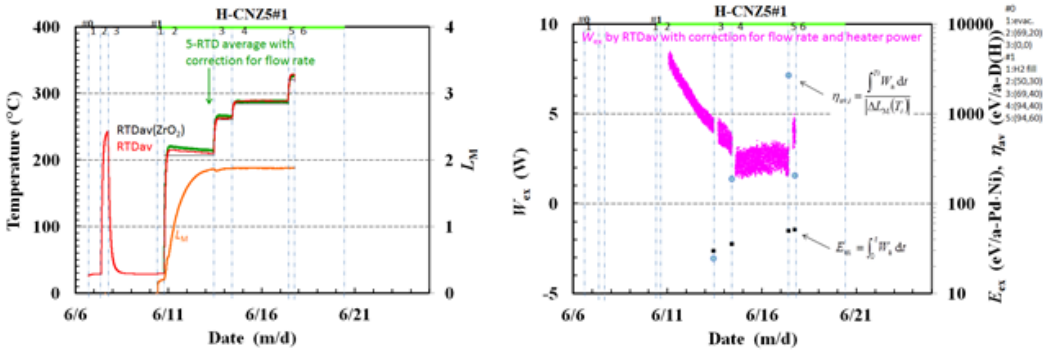

(a) **(b)**

Figure 7. Figures similar to Fig. 6 for CNZ5#1 run.

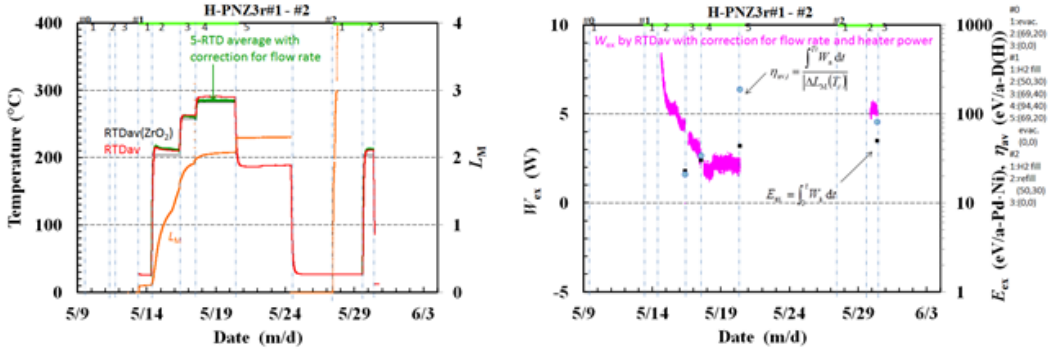

(a) **(b)**

Figure 8. Figures similar to Fig. 6 for PNZ3r#1 - #2 runs.

amount of material in the $NiZr_2$ phase was observed in the STEM/EDS pictures. The reason has not been determined yet.

4.2.3. *PNZ3r*

The same variables for PNZ3 and CNZ5 are plotted in Fig. 8(a) and (b) for the PNZ3r sample. This sample was re-calcined after finishing the PNZ3#4 run in air at a temperature of 450°C for 200 h, which caused a drastic change in the absorption property as discussed in Section 4.1.2. The absorption properties both at RT and in the elevated temperature phases are very similar to those in the CNZ5#1 run shown in Fig. 7. However, the evolution of $L_{\rm M}$ in the PNZ3r#1 run is shifted to the high temperature side by about 50°C compared with that in the CNZ5#1. The non-zero value of $L_{\rm M}$ in the PNZ3r#1-1 is decreased, and the increase of $L_{\rm M}$ still continues in the PNZ3r#1-4 phase. This shift might be suggesting the mechanism of hydrogen absorption by these materials at the elevated temperatures; absorption by Ni with catalysis by Pd or Cu, or contribution of the hydrogenation reaction (6). It is not clear at the moment.

This sample also generates excess power of up to 8 W, with $\eta_{{\rm av},j}$ ranging from 2.1×10^1 to 1.9×10^2 eV/atom-H and $E_{\rm ex}$∼5.0×10^1 eV/atom-M (5.0 MJ/mol-M) at the end of the #2 run. The values are very modest, though not explainable by any known chemical reaction energy [8].

At the end, it is noted that the abrupt increase in $L_{\rm M}$ at PNZ3r#2-1 phase is due to sealing failure at the chamber flange.

5. Summary

Hydrogen isotope absorption by nickel-based binary nano-composite samples has been examined in a collaborative work of the NEDO new MHE (metal hydrogen energy) project. The samples tested so far include $Pd_{0\ 044}Ni_{0\ 31}Zr_{0\ 65}$ ("PNZ3" and re-calcined "PNZ3r") and $Cu_{0\ 044}Ni_{0\ 31}Zr_{0\ 65}$ ("CNZ5"). Material characterization by XRD and STEM/EDS has revealed the existence of crystalline phases of $NiZr_2$, ZrO_2, etc., and binary-nano-particle structure of Pd/Ni and Cu/Ni in ZrO_2 supporter. The results obtained in the absorption runs are summarized in Table 3.

The virgin PNZ3 sample showed very strong absorption with rather large heat output in the #1-1 phase at RT, $L_{\rm M}$∼3.3 and $\eta_{\rm av}$∼0.6 eV/D, while in the #n-1 (n >1) phases after degassing process following elevated temperature runs, $L_{\rm M}$∼1.7 and $\eta_{\rm av}$∼0.4 eV/D. The difference could be due to the contribution of ZrH_2 formation in the former phase. On the other hand, the CNZ5 sample and the PNZ3r sample showed very little absorption but with comparable

Table 3. Summary of the results in comparison with those published earlier.

Sample	Room temp.				Elevated temp.		Ref.
	#1		#2,#3,...		L_M at 200°C/hump on RTD	Excess power	
	L_M	η(eV/a-D(H))	L_M	η(eV/a-D(H))			
CNS2	0	–	∼0	–	0.9/hump	10 W (TC2)	[12]
PS3	2	0.7	0.7	0.4	–	∼0	
PNZt	(1)	2	2	0.4	–	6 W /9 W (TC2/RTD)	[10]
CNZt	0.2	0.4	0.15	0.2	1.6/hump	5 W(TC2)	[10]
CNZtr	0.15	∼0	0.15	∼0	2.0/hump	∼0	
PNZ3	3.4	0.6	1.6	0.4	–	10 W (RTD)	This paper
PNZ3r	0.1	0.6	–	–	2.0/hump	8 W (RTD)	This paper
CNZ5	0.2	0.5	–	–	1.9/hump	8 W (RTD)	This paper
PNZ4	3.5	0.6	1.7	0.4	–	(Malfunctioning)	

η_{av}, L_M∼0.2 and η_{av}∼0.5 – 0.6 eV/H at RT. Both the CNZ5 and PNZ3r samples at temperatures around 200°C showed strong absorption with L_M∼2. To determine whether a nuclear process is involved or not, the amount of $NiZr_2$ in the virgin PNZ3 and the virgin CNZ5 samples, and the exact amount of $NiZrH_{2\ 5}$ in the samples in CNZ5#2-1 phase and PNZ3r#2-1 phases have to be established.

All samples at elevated temperatures (200–300°C) showed anomalous heat evolution: excess power W_{ex}∼5–10 W for several days, corresponding to excess energy E_{ex}∼5 keV/atom-D(H) = 0.5 GJ/mol-D(H). This could be the basis for carbon-free energy devices without hard radiation. However, since in practical applications the excess power must continue for an extended time (months or years), further effort to find better materials and better operating conditions is indispensable.

Acknowledgements

Some of the authors, A. K., A. T., and Y. F. are grateful for Mr. T. Yokose for his assistance in performing the STEM/EDS analysis.

References

[1] F. Celani, E.F. Marano, B. Ortenzi, S. Pella, S. Bartalucci, F. Micciulla, S. Bellucci, A. Spallone, A. Nuvoli, E. Purchi, M. Nakamura, E. Righi, G. Trenta, G.L. Zangari and A. Ovidi, Cu–Ni–Mn alloy wires, with improved sub-micrometric surfaces, used as LENR device by new transparent, dissipation-type, calorimeter, *J. Condensed Matter Nucl. Sci.* **13** (2014) 56–67.

[2] F. Piantelli, Nichenergy, http://e-catsite.com/2012/06/15/piantelli-moves-closer-to-commercialization/ .

[3] A. Rossi, Leonardo Corporation, http://ecat.com/ .

[4] G. Levi, E. Foschi, B. Höistad, R. Pettersson, L. Tegner and H. Essen, http://www.sifferkoll.se/sifferkoll/wp-content/uploads/2014/10/LuganoReportSubmit.pdf .

[5] A.G. Parkhomov, *Int. J. Unconventional Sci.* **6**(2) (2014) 57–61, ibid. **7**(3) (2015) 68–72, ibid. **8**(3) (2015) 34–39.

[6] S. Jiang, http://ja.scribd.com/doc/267085905/New-Result-on-Anomalous-Heat-Production-in-Hydrogen-loaded-Metals-at-High-Temperature (2015).

[7] J. Cole, http://www.lenr-coldfusion.com/2015/04/16/experiment-generates-apparent-excess-heat/ (2015).

[8] A. Takahashi, A. Kitamura, K. Takahashi, R. Seto, T. Yokose, A. Taniike and Y. Furuyama, Anomalous heat effects by interaction of nano-metals and D(H)-gas, *Proc. ICCF20*, *J. Condensed Matter Nucl. Sci.* **24** (2017).

[9] For example, A. Kitamura, A. Takahashi, R. Seto, Y. Fujita, A. Taniike and Y. Furuyama, Brief summary of latest experimental results with a mass-flow calorimetry system for anomalous heat effect of nano-composite metals under D(H)-gas charging, *Current Sci.* **108**(4) (2015) 589–593.

[10] Y. Iwamura, T. Itoh, J. Kasagi, A. Kitamura, A. Takahashi and K. Takahashi, Replication experiments at Tohoku university on anomalous heat generation using nickel-based binary nanocomposites and hydrogen isotope gas, *Proc. ICCF20*, *J. Condensed Matter Nucl. Sci.* **24** (2017).

[11] A. Kitamura, E.F. Marano, A. Takahashi1, R. Seto, T. Yokose, A. Taniike and Y. Furuyama, Heat evolution from zirconia-supported Ni-based nano-composite samples under exposure to hydrogen isotope gas, *Proc. JCF* **16** (2016) 1–16.

[12] P. Dantzer, W. Luo, T.B. Flanagan and J.d. Clewley, Calorimetrically measured enthalpies for the reaction of H_2 (g) with Zr and Zr alloys, *Metallurgical Trans.* A **24A** (1993) 1471–1479.

[13] A. Kitamura, A. Takahashi, R. Seto, Y. Fujita, A. Taniike and Y. Furuyama, Effect of minority atoms of binary ni-based nano-composites on anomalous heat evolution under hydrogen absorption, *J. Condensed Matter Nucl. Sci.* **19** (2016) 1–10.